Journal of Solid State Chemistry 184 (2011) 391–400

Contents lists available at ScienceDirect

Journal of Solid State Chemistry

journal homepage: www.elsevier.com/locate/jssc

Room temperature ferromagnetism in undoped and Fe doped ZnO nanorods: Microwave-assisted synthesis

Mukta V. Limaye [a], Shashi B. Singh [a,1], Raja Das [b], Pankaj Poddar [b], Sulabha K. Kulkarni [c,*,2]

[a] DST unit on Nanoscience, Department of Physics, University of Pune, Pune 411007, India
[b] Physical & Materials Chemistry Division, National Chemical Laboratory, Pune 411 008, India
[c] DST unit on Nanoscience, Indian Institute of Science Education and Research, Pune 411021, India

ARTICLE INFO

Article history:
Received 20 July 2010
Received in revised form
6 October 2010
Accepted 7 November 2010
Available online 2 December 2010

Keywords:
Diluted magnetic semiconductors
Nanostructures
ZnO

ABSTRACT

One-dimensional (1D) undoped and Fe doped ZnO nanorods of average length ~1 μm and diameter ~50 nm have been obtained using a microwave-assisted synthesis. The magnetization (M) and coercivity (H_c) value obtained for undoped ZnO nanorods at room temperature is $\sim 5 \times 10^{-3}$ emu/g and ~150 Oe, respectively. The Fe doped ZnO samples show significant changes in M –H loop with increasing doping concentration. Both undoped and Fe doped ZnO nanorods exhibit a Curie transition temperature (T_c) above 390 K. Electron spin resonance and Mössbauer spectra indicate the presence of ferric ions. The origin of ferromagnetism in undoped ZnO nanorods is attributed to localized electron spin moments resulting from surface defects/vacancies, where as in Fe doped samples is explained by F center exchange mechanism.

1. Introduction

Diluted magnetic semiconductors (DMS) [1,2] have attracted much attention, due to the possibility of using spin degrees of freedom and charge manipulation in these materials [3,4]. DMS materials are believed to be an ideal candidate for spintronics, since they can be easily integrated into microelectronic technology [4,5]. The main challenge is to develop materials with T_c at or above room temperature that can lead to establishment of spintronics as a practical technology. Considerable work has been carried out on transition metal doped semiconductor oxide materials like ZnO, SnO_2, TiO_2, etc. [6–9].

Among the various II–VI semiconductor oxide materials, ZnO is one of the materials at the focus of much attention. Sluiter et al. [10] have theoretically predicted that the transition metal ions (TM=Ti, V, Cr, Mn, Fe, Co, Ni, Cu) doped ZnO is ferromagnetic at room temperature. A number of experimental reports are available on ZnO doped with transition metal ions with few conflicting reports [6,11–26]. Giant magnetic moment has been observed in $Zn_{0.96}Co_{0.04}O$ films (6.1 μ_B per Co atom) with T_c~790 K by Song et al. [22]. In case of $Zn_{0.95}Cu_{0.05}O$ films magnetic moment observed is 1.45 μ_B per Cu atom with T_c greater than 300 K [16]. Amine capped 0.20% Mn doped ZnO nanocrystals show magnetic moment 1.22 μ_B per Mn^{2+} ion with T_c well above 350 K [20]. Wang et al. [21,23] have synthesized Co and Cu doped ZnO nanocrystals. The behavior of Co doped ZnO was investigated using XPS, EELS, HRTEM and Raman spectroscopy which led them to conclude that ferromagnetism existed in Co doped ZnO is intrinsic property [21]. In Cu doped ZnO nanocrystals, spin split acceptor impurity model was proposed to explain ferromagnetism. They claim that the spatial inhomogeneity associated with spinodal decomposition can strongly affect the ferromagnetism [23]. Zhang et al. [25] have reported the evidence of intrinsic ferromagnetism in individual ZnO nanoparticles doped with transition metal ions. Using various characterization techniques they showed that ZnO nanoparticles have intrinsic ferromagnetism when doped with cobalt, but not when doped with iron [25]. It is observed that as compared to any other transition metal ions, Fe doped samples show lower magnetic moment. In $Zn_{0.96}Fe_{0.04}O$ thin films magnetic moment observed is ~0.15 μ_B with T_c~400 K [12]. The 10% Fe doped ZnO nanocrystals of ~7 nm show 0.05 μ_B magnetic moment with T_c greater than 450 K [13]. However, co-doped sample $Zn_{0.94}Fe_{0.05}Cu_{0.01}O$ bulk sample shows magnetic moment 0.75 μ_B per Fe atom with T_c~550 K [11].

New complexicity has been introduced in this field by the observation of room temperature ferromagnetism in various undoped, nonmagnetic selenides [27,28], sulphides [29] nitrides [29] and oxides [30–34]. Garcia et al. [31] have demonstrated magnetic properties of the chemically synthesized ZnO nanoparticles capped with three different organic molecules (thiols, amine and TOPO). The thiol capped pure ZnO nanoparticles

* Corresponding author. Fax: +91 020 25898022.
E-mail address: s.kulkarni@iiserpune.ac.in (S.K. Kulkarni).
[1] Currently at International Centre for Materials Science (ICMS) Jawaharlal Nehru Centre for Advanced Scientific Research, Bangalore-560064, India.
[2] Currently at Banasthali University, P. O. Banasthali Vidyapith-304022 (Rajasthan).

0022-4596/$ - see front matter © 2010 Published by Elsevier Inc.
doi:10.1016/j.jssc.2010.11.008

(~10 nm) show highest value of room temperature ferromagnetism (~2×10^{-3} emu/g) as compared to the other two. They proposed that the modification in the electronic structure due to electrons/holes trapped at defects, induces ferromagnetism in ZnO and the magnetic properties of nanoparticles strongly depend on the preparation method [31]. Sundaresan et al. [32] observed RTFM in uncapped nonmagnetic oxide nanoparticles such as CeO_2, Al_2O_3, ZnO, In_2O_3 and SnO_2. They attributed the origin of ferromagnetism to the exchange interaction between localized electron spins resulting from oxygen vacancies present on the surface of nanoparticles. The MgO powders prepared by sol–gel method also exhibit RTFM where as bulk MgO is diamagnetic [34]. The authors attribute the origin of RTFM to the Mg vacancies. Although large number of experimental and theoretical reports are available, the origin of ferromagnetism in undoped and doped DMS materials is under debate.

To utilize semiconductor nanostructures as building blocks of functional nanodevices, it is important to synthesize one-dimensional (1D) nanostructures such as rods, wires and tubes, and study the effect of dimensionality on magnetism [35]. In spite of having microscopic lengths, 1D nanostructures are of great research interest due to their diverse optical and electrical properties arising due to quantum confinement effects in the radial direction. In this regard, many researchers try to synthesize transition-metal doped semiconductor nanostructures like nanowires, nanorods [36–44] as the theoretical work predicted that these materials could exhibit high Curie temperatures (T_c) [45]. Philipose et al. [36] observed T_c~400 K in Mn doped ZnO nanowires with 1.2 μ_B magnetic moment per Mn atom. Also, the nanowires of (Ga,Mn)As and GaN:MnAlSi show enhancement in T_c as compared to bulk [37,38]. In Co doped ZnO nanowires Jian et al. [39] have provided connection between structural order and ferromagnetism. Enhanced magnetism was observed in $Zn_{0.98}Co_{0.02}O$ nanowires (average diameter ~45 nm and length ~2–6 μm) as compared to $Zn_{0.98}Co_{0.02}O$ thin film [46]. It is attributed to the combined effect of 1D size and homogeneous doping of Co in nanowires. Wang et al. [40] have synthesized Co doped ZnO nanorods and using micro-Raman spectroscopic technique they have detected hidden secondary phase. The origin of the ferromagnetism was probably due to the presence of the mixed cation valence of Co via a *d–d* double-exchange mechanism rather than the real doping effect. Wang et al. [43] demonstrated the scaling of dopant states of individual semiconducting nanostructures by chemically resolved electron energy-loss spectroscopy (EELS) in individual Co doped ZnO nanorod. The origin of room temperature ferromagnetism occurring in Co doped ZnO structures was explained by carrier mediated process [43]. To the best of our knowledge there are very few reports available on Fe doped 1D nanostructures with systematic magnetic study with respect to doping concentration. Uum et al. [41] have synthesized Fe doped ZnO nanorods using hydrolysis method with diameter of 30 nm and length of 300 nm. They observed a shift in the band gap by Fe doping and studied the magnetic behavior of the samples using Mössbauer spectroscopy and vibrating sample magnetometer. It was also observed that 5 wt% Fe doped sample shows RTFM (weak sextet and central doublet at room temperature) and it vanishes above that. The coercivity value obtained for 5 wt% Fe doped sample was ~210 Oe [41]. The electronic structure studies of Fe doped ZnO nanorods synthesized by co-precipitation method indicate that Fe ions replace Zn ions in the ZnO matrix [42]. The Fe *K-edge* studies demonstrate that Fe is present in mixed valence state (Fe^{3+}/Fe^{2+}). Kumar et al. [47] have observed RTFM in chemically synthesized pure ZnO nanorods of 200 nm diameter and 550 nm length. The saturation magnetization observed is ~2×10^{-3} emu/g and coercivity ~102 Oe. They have attributed the origin of RTFM to Zn vacancies. Since nanostructure materials are ideal for optoelectronic and nanoelectronic devices, systematic optical and magnetic studies of undoped and Fe doped ZnO 1D nanostructures by varying Fe doping concentration are of high interest. However, preparation of symmetrical nanostructures with high aspect ratio is challenging.

The morphology of nanomaterials highly depends on the synthesis method. ZnO nanorods have been obtained earlier using physical and chemical methods such as pulsed laser deposition (PLD) [48], chemical vapor deposition (CVD) [49], templated electrosynthesis [50], thermal decomposition [51], etc. However, compared to these methods, microwave-assisted technique discussed here offers great advantages such as short synthesis time, high yield, low cost and simple procedure. Therefore, it is used to synthesize materials like CdS, CdSe, ZnSe, ZnS, etc. [52,53]. Furthermore, with microwave-assisted technique, it can be possible to scale-up [52].

In this communication, we report the synthesis of undoped, uncapped ZnO nanorods by rapid and simple microwave-assisted route. The RTFM is observed in the sample due to intrinsic defects present in the ZnO nanorods and not because of the magnetic impurity or capping molecules. Further we have doped the ZnO with Fe by varying the Fe doping concentration without altering the morphology. The effect of doping concentration on the magnetic and optical properties was investigated.

2. Experiment

2.1. Synthesis of undoped and Fe doped ZnO nanorods

Aqueous solutions of (0.1 M) $ZnSO_4$ and (0.1 M) NaOH were mixed in a 250 ml round-bottom flask and kept in a microwave system. The microwave chamber has the dimensions of 360 mm × 210 mm × 430 mm and maximum deliverable power output is 700 W. The samples were prepared using 140 W (20%) irradiation power. The reaction product in the form of a precipitate was centrifuged, washed with distilled water and dried in vacuum. The final white product was collected for characterization.

The synthesis procedure for Fe doped ZnO nanorods is same as mentioned above. Only change is that while preparing doped ZnO nanorods, $FeSO_4$ was added in different molar amounts.

2.2. Characterization

The atomic absorption spectroscopy was carried out on a VARIAN spectrometer to check the actual atomic% of Fe doping in ZnO sample. The phase of the sample was determined by X-ray diffraction (XRD) using a Bruker D8 Advance diffractometer with Cu $K\alpha$ radiation (1.54 Å). The morphology of sample was observed using a JEOL-6360 scanning electron microscope (SEM). The transmission electron microscopy (TEM) was carried out using TECHNAI 20 G2 transmission electron microscope from FEI operated at an accelerating voltage of 200 keV. The sample for TEM analysis was prepared on carbon coated copper grids by placing drop of dilute solution prepared by dispersing the powder in dimethyl formamide (DMF). The UV–vis absorption spectra of the liquid samples were recorded using a Perkin Elmer Lambda-950 spectrometer. Mössbauer measurements were performed on constant acceleration Wissel ^{57}Fe Mössbauer spectrometer using 50 mCi ^{57}Co:Rh source and data was analyzed using WinNormos-IGOR software. The electron spin resonance (ESR) spectra were recorded at room temperature and at 77 K on a VARIAN E112 spectrometer using 9.1 GHz X-band frequency. The photoluminescence (PL) spectra of powder samples were acquired on a Perkin Elmer Lambda-55 spectrometer at room temperature. The magnetic measurements were performed on a Lakeshore 7307 model

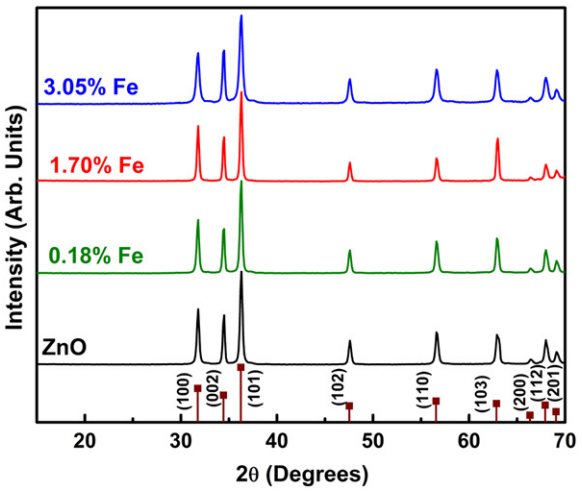

Fig. 1. XRD pattern of ZnO and Fe (0.18 at%, 1.70 at% and 3.05 at%) doped ZnO with standard wurtzite peak position of bulk ZnO.

vibrating sample magnetometer (VSM) as well as using the Physical Property Measurement System (PPMS) from Quantum Design Inc. San Diego, USA equipped with a VSM operating at 40 Hz and 7 T superconducting magnet and rms sensitivity of $< 10^{-6}$ emu.

3. Results and discussion

Purity and actual Fe doping percentage in the ZnO sample is checked by atomic absorption spectroscopy (AAS). The AAS study shows that there are no unintentional magnetic impurities present in the samples. The actual atomic percentage of iron in all Fe doped samples are 0.18%, 0.96%, 1.70% and 3.05%. The structure of the undoped and Fe doped ZnO samples is determined by XRD. In Fig. 1, we have compared the powder XRD pattern of undoped and Fe (0.18, 1.70 and 3.05 at%) doped ZnO. The XRD patterns of all the samples are in good agreement with the wurtzite structure of bulk ZnO (JCPDS Card No. 80-0075). For the sake of comparison the standard peak positions of bulk wurtzite ZnO are also shown. No indication of any secondary phase of iron is found. Fig. 2(a)

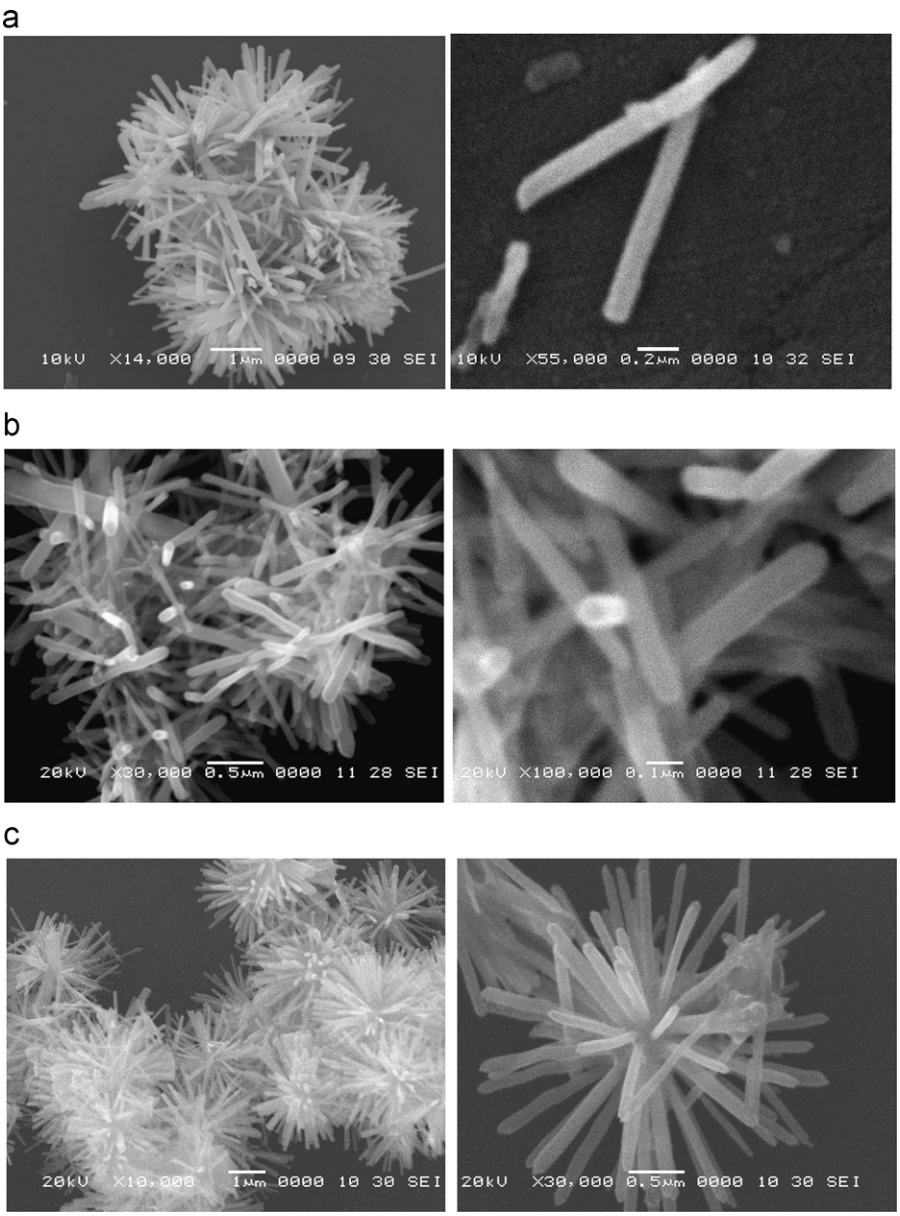

Fig. 2. SEM image of (a) ZnO, (b) 0.18 at% Fe doped ZnO and (c) 1.70 at% Fe doped ZnO nanorods at different magnification.

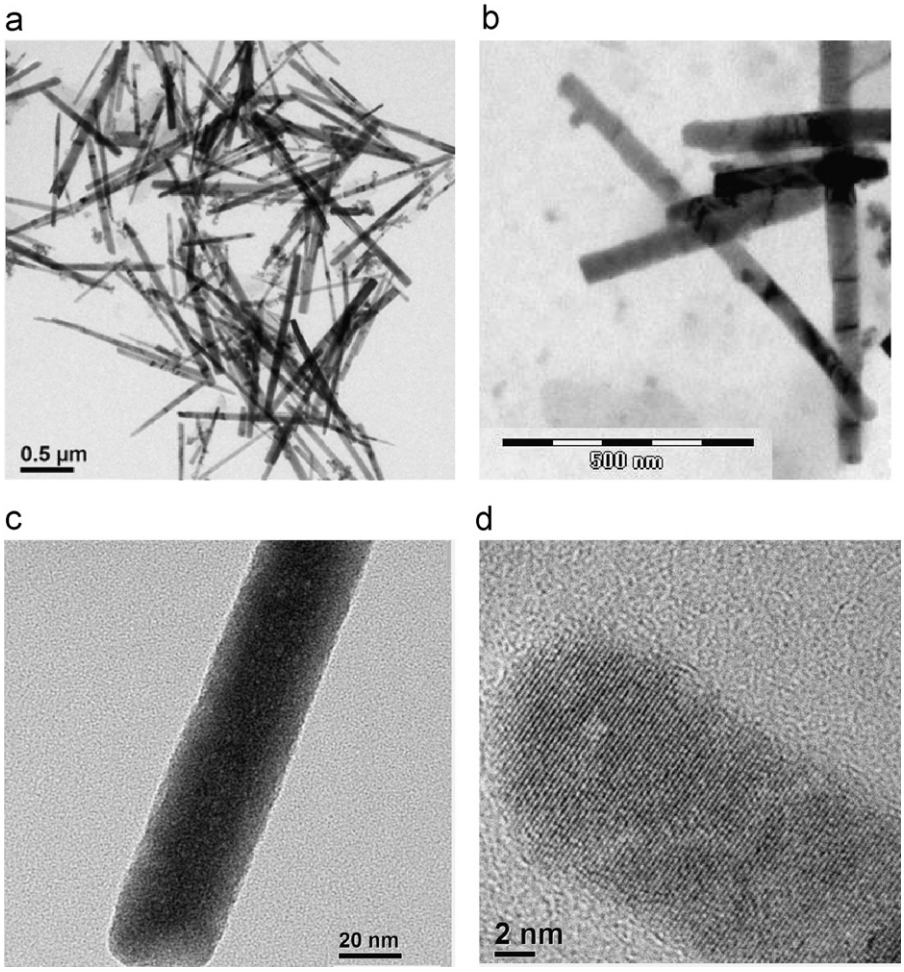

Fig. 3. TEM images of (a) ZnO and (b) 0.18 at% Fe doped ZnO. (c) and (d) HRTEM images of 0.18 at% Fe doped ZnO.

shows the SEM image of undoped ZnO sample recorded at different magnifications. The formation of rods with large aspect ratio can be clearly seen in the SEM images with average length ~1 μm and diameter in the range of ~50 nm. Fig. 2(b) and (c) show the SEM images of Fe doped ZnO nanorods with different doping concentrations (0.18 and 1.70 at%). The Fe doped samples also show rod-like structure with nearly the same dimensions. We have also performed TEM analysis of the same samples. Fig. 3(a) and (b) are the TEM images of undoped ZnO and (0.18 at%) Fe doped ZnO. The TEM results also confirm the rod-like morphology as seen in the SEM images. HRTEM images of 0.18 at% Fe doped ZnO are shown in Fig. 3(c) and (d). The *d* spacing of the 0.18 at% Fe doped ZnO sample calculated from the HRTEM image is 0.16 nm which matches well with *d* spacing of (1 1 0) plane of ZnO.

UV–vis absorption spectra of all the undoped and Fe doped ZnO nanorods were recorded (Fig. 4). In all the samples absorption peak is observed at ~365 nm, blue shifted as compared to that of bulk (~377 nm). Long tailing observed in all the samples indicates the formation of rod-like structure as it is common in high aspect ratio nanostructures [52,53].

The local environment and charge state of Fe in ZnO is determined using Mössbauer spectroscopy and electron spin resonance. Fig. 5 show the room temperature Mössbauer spectra of undoped ZnO and Fe doped (0.18, 1.70 and 3.05 at%) ZnO nanorods. In 0.18 at% Fe doped ZnO sample, no signature of ^{57}Fe is observed, due to small amount of ^{57}Fe. The 1.70 at% Fe doped ZnO sample shows a broad doublet at 300 K, which we have not attempted to fit, indicating presence of Fe^{3+} ions. The doublet is

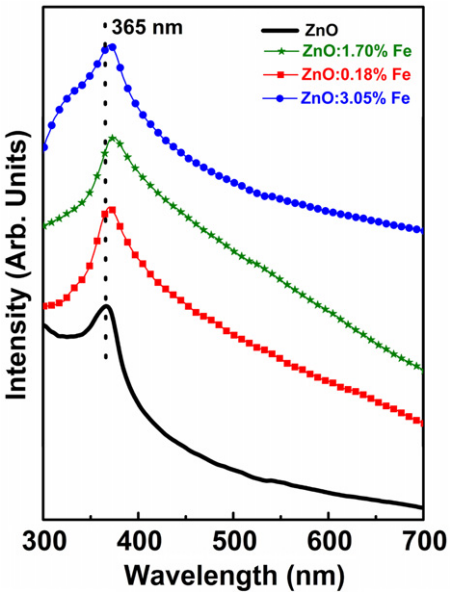

Fig. 4. UV–vis absorption spectra of ZnO, and Fe (0.18 at%, 1.70 at% and 3.05 at%) doped ZnO nanorods.

observed for 3.05 at% Fe doped ZnO sample. The fitting of the data indicates presence of two doublets with isomer shift (IS) 0.37 and 0.41 mm/s and quadruple splitting (QS) 0.51 and 0.83 mm/s,

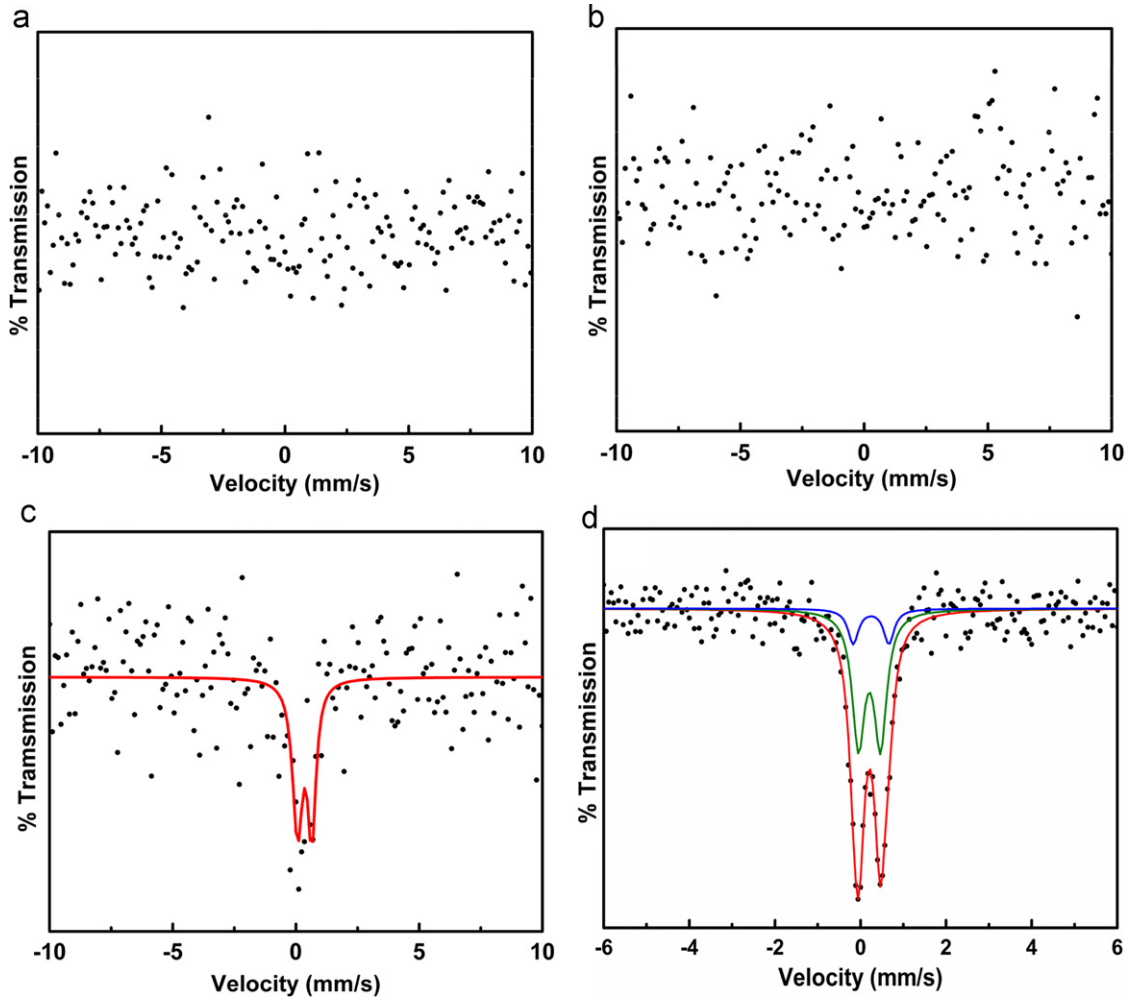

Fig. 5. Room temperature Mössbauer spectra of (a) ZnO, (b) 0.18 at%, (c) 1.70 at% Fe and (d) 3.05 at% Fe doped ZnO nanorods.

respectively. The values of IS values indicate the presence of high spin Fe^{3+} ions [7,13,54] in two different environments. Similar room temperature Mössbauer spectra were observed by Singhal et al. [54] in case of iron doped In_2O_3 nanoparticles.

The ESR measurements of undoped and Fe doped samples are carried out at room temperature as well as at 77 K. The room temperature ESR spectra of undoped and Fe doped ZnO nanorods are shown in Fig. 6. Undoped sample shows very weak (magnified 80 times compared to 3.05 at% Fe doped sample) and broad signal. Such a broad signal is also observed for undoped CdSe and GaN nanoparticles [28,30]. Also ESR measurements have been reported in the literature for ZnO powders, single crystals and nanocrystals [55–57]. The $g \sim 2.013$ value was assigned to zinc vacancies [55] and $g \sim 1.96$ to oxygen related defects [56]. Thus, the origin of broad ESR signal in undoped ZnO nanorods can be ascribed to zinc and oxygen defects/vacancies. In Fig. 6, Fe doped ZnO samples show broad signal with g_{eff} value ~ 2.11 (0.18 at% Fe), ~ 2.10 (1.70 at% Fe) and ~ 2.01 (3.05 at% Fe) at room temperature. The broad signal observed in 0.18 and 1.70 at% Fe doped sample can be due to superposition of two overlapping signals. It is attributed to the exchange couple interaction between iron ions [54]. Similar broad ESR signal was observed in Fe doped ZnO nanocrystals at 300 K by Karmakar et al. [13]. In case of 3.05 at% Fe doped sample relatively sharp ESR signal with $g \sim 2$ is observed possibly due to strong exchange couple interaction between iron ions.

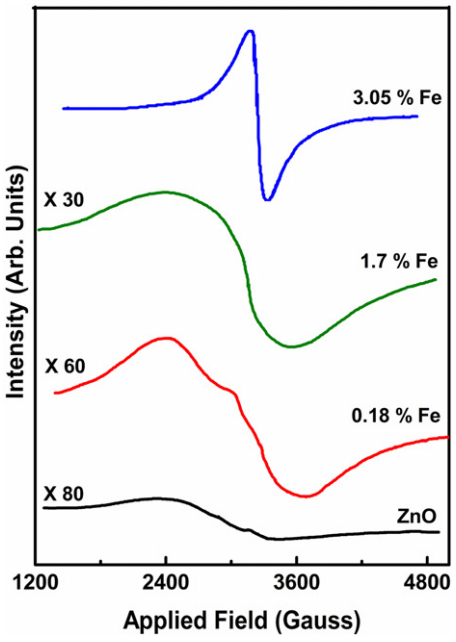

Fig. 6. Room temperature ESR spectra of undoped and Fe doped (0.18%, 1.70% and 3.05%) ZnO nanorods.

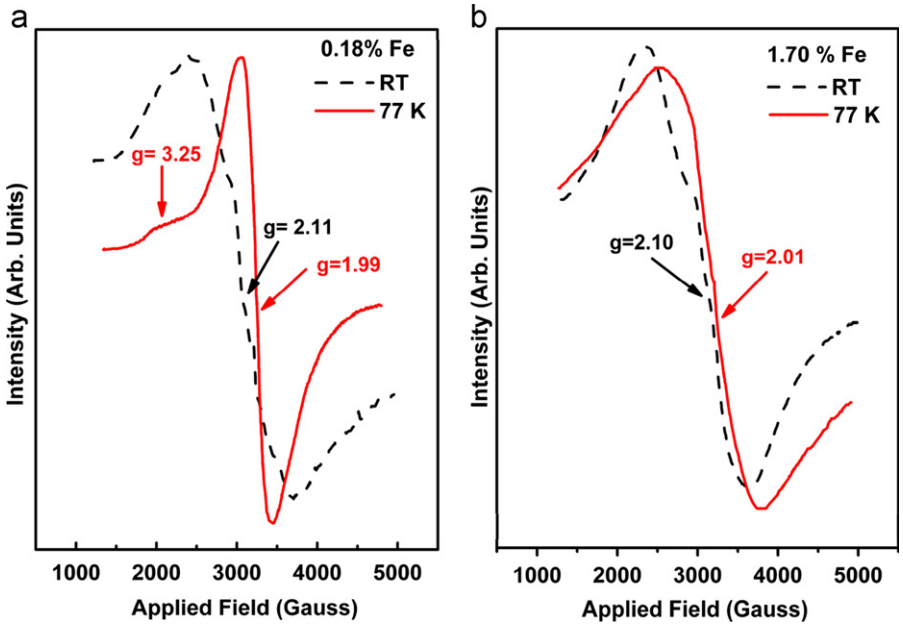

Fig. 7. ESR spectra of (a) ZnO doped with (0.18 at%) Fe recorded at room temperature and at 77 K. (b) ZnO doped with (1.70 at%) Fe recorded at room temperature and at 77 K.

Fig. 7(a) and (b) shows ESR spectra of 0.18 and 1.70 at% Fe doped ZnO nanorods at 77 K, respectively. For the sake of comparison room temperature ESR spectra of both the samples are also included. Low temperature (77 K) ESR signal of 0.18 at% Fe doped sample shows two distinct peaks at $g \sim 3.25$ and at $g \sim 1.99$. Based on the spin-Hamiltonian formalism [58], the resonance peak at higher g value can be assigned to the Fe^{3+} ions in a distorted local lattice position of surrounding oxygen ions. The peak at $g \sim 1.99$ can be assigned to interacting ferric ions occupying nearly symmetric local lattice position [59]. The 1.70 at% Fe doped sample does not show two distinct ESR signals even at 77 K. Such changes in the resonance signal by increasing Fe concentration is a clear indication of strongly interacting iron ions occupying the lattice position with no local lattice distortion around surrounding oxygen ions [60]. Thus ESR measurements have shown a signature of coexistence of strong and weak exchange coupled interactions in Fe doped ZnO nanorods.

The electronic structure of the samples is studied using photoluminescence analysis. Fig. 8 shows the photoluminescence spectra of undoped and Fe doped (0.18, 1.70 and 3.05 at%) ZnO nanorods sample. All the samples were excited with $\lambda_{ex} = 330$ nm. The spectra of all the samples show broad emission in the visible region. The signal observed at ~411 nm is attributed to zinc vacancies [61]. Other peaks observed at ~428 nm can be ascribed to divalent zinc vacancy and ~471 nm to intrinsic defects such as interstitial zinc and oxygen [61,62]. The small peak observed at ~447 nm corresponds to the transition of electrons from shallow donor levels of oxygen vacancies to the valence band and the peak at ~461 nm is assigned to electronic transition from shallow donor levels of zinc interstitial to the valence band [63]. The typical green emission peak observed at ~520 nm is from the positively charged single ion oxygen vacancy present on the surface of the nanoparticles [64,65]. All the above peaks are observed in undoped as well as Fe doped ZnO nanorod samples. Presences of zinc and oxygen related defects observed in the photoluminescence study supports the origin of ESR signal in undoped ZnO nanorods. With increasing Fe doping concentration, quenching of the photoluminescence intensity is observed. It clearly indicates that photoexcited electrons are preferentially transferred to the iron ion induced trap centers, resulting into the quenching of luminescence [60].

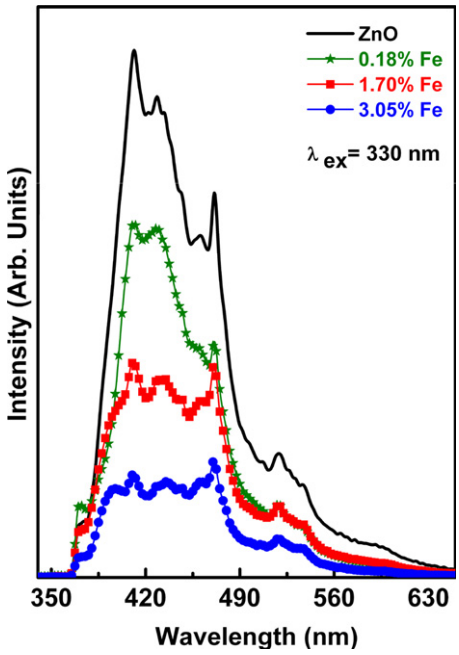

Fig. 8. Photoluminescence spectra of ZnO, and Fe (0.18 at%, 1.70 at% and 3.05 at%) doped ZnO nanorods.

In Fig. 9 we have shown the magnetic measurements of undoped, uncapped ZnO nanorods recorded at 300 K. We observed the room temperature ferromagnetism (RTFM) in undoped ZnO nanorods with magnetization (M) $\sim 5 \times 10^{-3}$ emu/g and coercivity (H_c) ~150 Oe at an applied field of 5000 Oe. The observed M value here for ZnO nanorods is higher than the observed M values for pure, spherical ZnO nanoparticles and pure ZnO nanorods [31,32,47,66]. Garcia et al. [31] have observed RTFM in thiol capped ZnO spherical nanoparticles (~10 nm). They observed magnetization $\sim 2 \times 10^{-3}$ emu/g at 10 kOe and it depends on the type of capping molecules as well as synthesis method. Sundaresan et al. [32] have observed RTFM in ~30 nm size uncapped, spherical ZnO

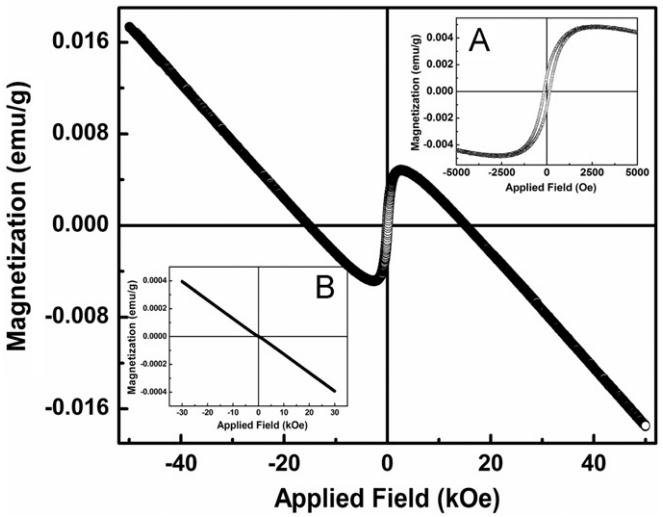

Fig. 9. Room temperature (300 K) magnetization curve of ZnO nanorods. Inset (A) expands the lower field region and inset (B) shows background signal.

nanoparticles with magnetization value $\sim 5 \times 10^{-4}$ emu/g at 2000 Oe. They proposed that the ferromagnetism is due to oxygen vacancies. Pure ZnO nanorods synthesized by chemical route show magnetization and coercivity $\sim 2-10^{-3}$ emu/g and 102 Oe, respectively, at 300 K [47]. Yan et al. [66] have observed RTFM in surfactant free ZnO pseudospherical structures. They observed the value of magnetization at 300 K is $\sim 1.5 \times 10^{-3}$ emu/g and coercivity is ~120 Oe at an applied field of 5 kOe. They attributed the origin of RTFM to defects. We also have not used any organic capping molecules for synthesis of ZnO nanorods, however magnetization value obtained here is higher as compared to any other reported value of undoped ZnO. The origin of RTFM here is associated with vacancies/defects present on the surface of undoped nanorods. The exchange coupling of localized spins present on the vacancies/defects at the surface of nanorods gives rise to resultant magnetization to the sample. The broad ESR signal of undoped nanorods (Fig. 6) is an indication of the exchange coupled interaction between the spins of surface vacancies/defects. The enhancement in the magnetic properties of ZnO nanorods is probably due to shape anisotropy. Such results are also observed in MnS nanostructures by Jun et al. [67].

Room temperature magnetic measurements of all the Fe doped ZnO samples are illustrated in Fig. 10(a) recorded at an applied field of 5000 Oe. Inset of Fig. 10(a) shows plot of magnetic moment per Fe atom vs. Fe doping concentration. It is observed that as Fe doping concentration increases magnetic moment decreases. Similarly, Parra-Palomino et al. [68] had observed decrease in magnetic moment in Fe doped ZnO nanocrystals as doping percentage increases from 0.05 to 0.08. Since saturation magnetization is not observed up to 5000 Oe, we have carried out the *M–H* measurements up to 50 kOe for 0.96 and 3.05 at% Fe doped samples at 300 K (Fig. 10(b) and (c)). However, up to 50 kOe also the magnetization shows continuous increase with an applied field in both the samples. The magnetization values observed at 50 kOe are ~0.06 and ~0.21 emu/g for 0.96 and 3.05 at% Fe doped samples, respectively. The coercivity value increases to ~160 Oe in 0.96 at% Fe doped sample compared to undoped ZnO (~150 Oe) and then goes down to ~45 Oe for 3.05 at% Fe doped sample. The changes in the *M–H* loop can be explained as the resultant magnetic contribution from orientation of the exchange coupled ferric ions. With the increase in Fe doping concentration the linearization of *M–H* loop also increases. It indicates that iron–iron superexchange dominates at higher Fe doping concentrations at 300 K [69]. Such

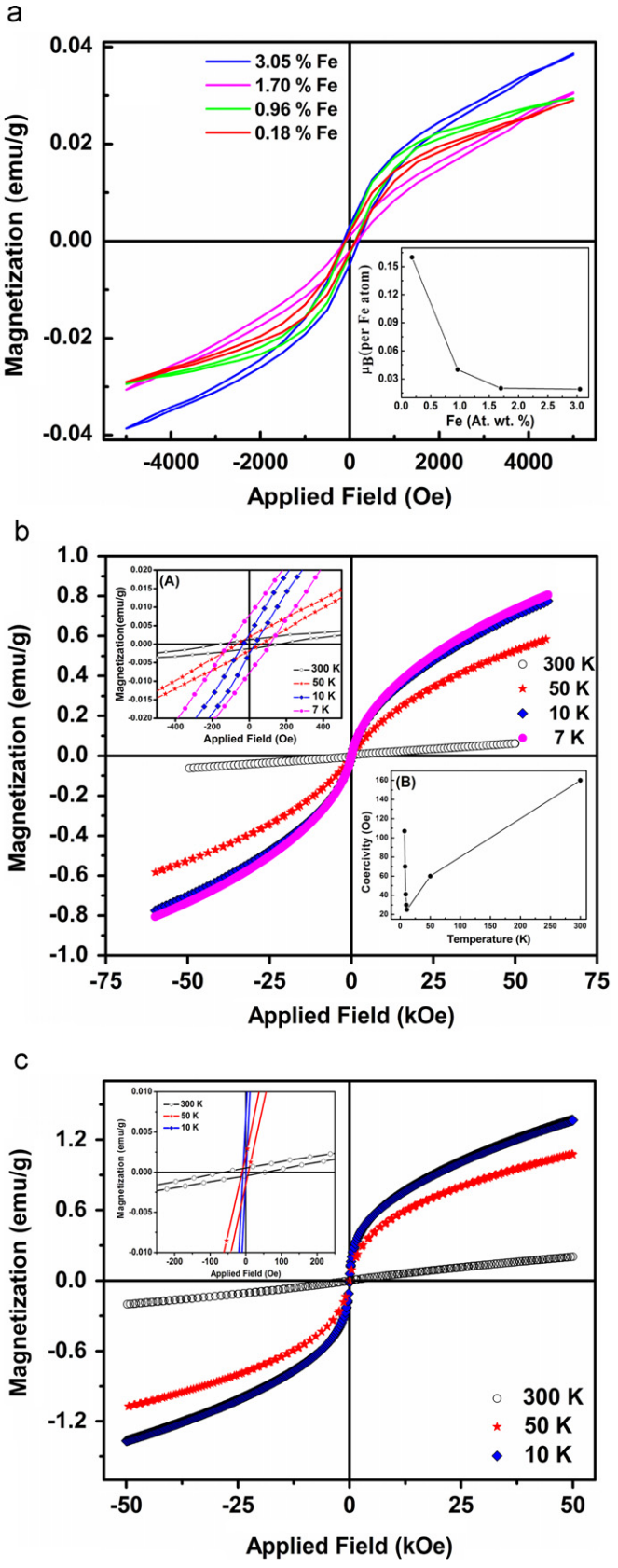

Fig. 10. Room temperature (300 K) magnetization curve of (a) Fe doped (0.18 at%, 0.96 at%, 1.70 at% and 3.05 at%) ZnO nanorods with subtracting background at an applied field of 5000 Oe. Inset shows plot of variation of μ_B per Fe atom with respect to Fe doping concentration. *M–H* loops recorded at different temperatures and at high magnetic field for (b) 0.96 at% Fe, Inset (A) expand the low field region. Inset (B) is the plot of coercivity vs. temperature. (c) 3.05 at% Fe. Inset expands the low field region.

Table 1
The observed magnetization and coercivity of undoped ZnO and Fe (0.96 at% and 3.05 at%) doped ZnO nanorods at different temperatures are given in table.

At 300 K				At 50 K			At 10 K			At 7 K		
Sample (at wt% (AAS) Fe) ZnO rods	M (emu/g)	H_c (Oe)	μ_B/Fe atom at 50 kOe	M (emu/g)	H_c (Oe)	μ_B/Fe atom at 50 kOe	M (emu/g)	H_c (Oe)	μ_B/Fe atom at 50 kOe	M (emu/g)	H_c (Oe)	μ_B/Fe atom at 50 kOe
0% Fe	0.005	150	–	–	–	–	–	–	–	–	–	–
0.96 % Fe	0.06	160	0.09	0.58	60	0.8	0.77	30	1.07	0.81	107	1.23
3.05 % Fe	0.21	45	0.1	1.08	10	0.51	1.37	5	0.65	–	–	–

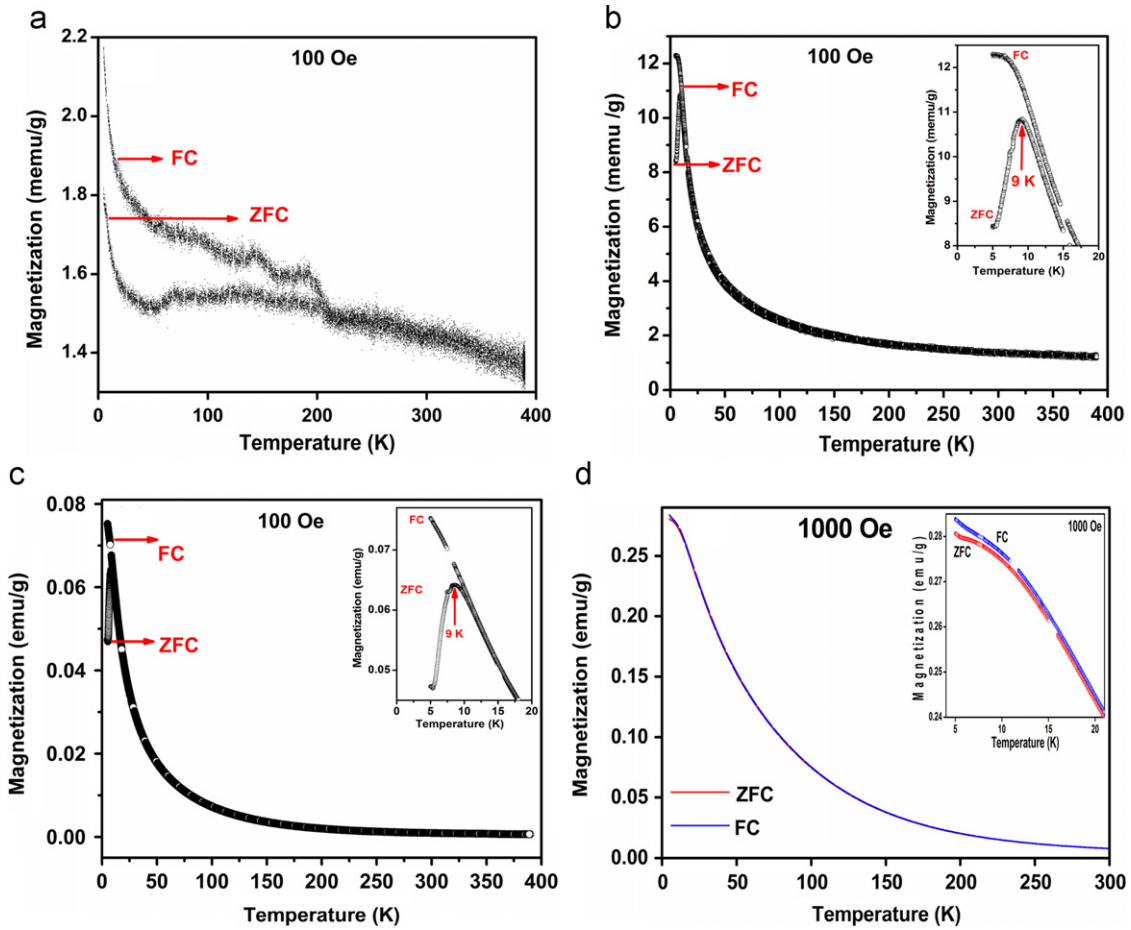

Fig. 11. ZFC–FC recorded at applied field of 100 Oe (a) undoped ZnO, (b) 0.96 at% Fe and (c) 3.05 at% Fe. Inset of (b) and (c) expand the low temperature region and (d) ZFC–FC recorded at an applied field of 1000 Oe for 3.05 at% Fe, inset expand low temperature region.

behavior of M–H loop was also observed in many Fe doped nanocrystals [6,54,68–71]. The M–H loops of 0.96 and 3.05 at% Fe doped ZnO nanorods at low temperatures start exhibiting nonlinearity and significant reduction is seen in the coercivity values from 300 to 10 K (Fig. 10(b) and (c)). Such changes are also observed in Fe doped $PbTiO_3$ nanocrystals [70] and Mn doped InP quantum dots [72]. The observed magnetization at 50 kOe and coercivity at different temperatures are tabulated in Table 1. The 0.96 and 3.05 at% doped samples show a coercivity of ~30 and ~5 Oe, respectively, at 10 K. The μ_B/Fe atom values decreases as Fe doping concentration increases from 0.96 to 3.05 at% at lower temperatures. (Table 1) It shows a signature of presence of some antiferromagnetic interactions in the sample [13,70,72,73]. Interestingly, below 9 K, distinct hysteretic response is observed for 0.96 at% Fe doped sample (Fig. 10(b), Inset A). The plot of coercivity with respect to temperature is shown in Fig. 10(b) Inset B. The M–H loop of 0.96 at% Fe doped ZnO (Fig. 10(b)) starts broadening with a coercivity of 70 Oe at 8 K and 107 Oe at 7 K. Further increase in coercivity below 9 K indicates the presence of surface spin canting effects.

The low temperature magnetic behavior is investigated by zero-field-cooled (ZFC) and field-cooled measurements. Fig. 11 shows ZFC–FC curves of samples (a) undoped ZnO, (b) 0.96 at% Fe and (c) 3.05 at% Fe doped ZnO nanorods recorded from 5 to 390 K temperature range. ZFC curve is obtained by initially cooling the sample from 300 to 5 K in the absence of magnetic field and heating up in 100 Oe field while recording magnetization. For the FC measurements, sample is cooled in the same field and magnetization is recorded while heating-up (FC). It is observed that Curie transition temperature (T_c) of undoped ZnO nanorods is above 390 K. FC curves of 0.96 and 3.05 at% Fe doped samples also show absence of Curie transition temperature (T_c) below 390 K. The cusp is observed in the ZFC curve at ~9 K in 0.96 and 3.05 at% Fe doped ZnO nanorods. It may appear due to various reasons. To verify

different possibilities we have checked the existence of any oxide phase of iron. XRD measurements carried out at room temperature show no evidence for the presence of possible oxide phase of iron. It rules out the possibility of presence of any other impurity phase in the sample. If any impurity phase is present in the sample it is below the detection limit of XRD.

The presence of superparamagnetism was checked by plotting M vs. H/T curves for the M–H data of 3.05 at% Fe sample recorded at different temperatures (Supporting information Fig. S1). For superparamagnetic systems M–H curves recorded at different temperatures should superpose in a plot of M vs. H/T [13,74]. It is observed that all the curves remain distinct. It rules out the possibility of presence of superparamagnetism.

Further we have carried out ZFC measurements at high magnetic field (1000 Oe) for 3.05 at% Fe doped ZnO sample shown in Fig. 11(d). It is observed that at higher magnetic field the meeting point of the ZFC and FC curves as well as cusp shift towards lower temperature value. As the samples are weakly ferromagnetic when higher magnetic field (1000 Oe) is applied all the spins get aligned in the direction of applied field giving rise to lowering of temperature. Similar results were observed by Karmakar et al. [13] in 10% Fe doped ZnO nanocrystals. They have attributed the cusp observed in ZFC measurements to transition from ferromagnetic to spin glass state. The existence of spin glass state was explained in terms of core–shell model for the spin structure.

In order to explain the origin of ferromagnetic contribution in Fe doped ZnO nanorods, we have employed F-center exchange (FCE) mechanism proposed by Coey et al. [7] in which exchange interaction of two iron ions through the F center (electron is trapped into the defects), is ferromagnetic in nature. This direct ferromagnetic coupling is also called as bound magnetic polaron [6,7,75,76]. In defect free Fe doped ZnO, Fe will go to the substitutional site. Its charge state shall be 2+. However, both ESR and Mössbauer measurements indicate incorporation of Fe^{3+} ions in our Fe doped ZnO nanorods. Due to charge mismatch of Fe^{3+} and Zn^{2+} more number of defects produced in the sample which can give rise to large number F centers. Ultimately, number of overlapping bound magnetic polarons increases. This mechanism leads to resultant ferromagnetic contribution in the Fe doped samples. In addition, Fe^{3+} is paramagnetic in nature, which contributes to give linearization to M–H loop. The number of F centers and interaction between two iron ions through F centers is highly dependent on the iron doping concentration [69]. As Fe doping concentration increases the antiferromagnetic (Fe^{3+}–O^{2-}–Fe^{3+}) exchange interaction [69,70] dominates the ferromagnetic interaction. The competition between the ferromagnetic and paramagnetic/antiferromagnetic exchange interactions will lead to the substantial changes in the observed M–H loop at room temperature. This mechanism is represented schematically in Fig. 12.

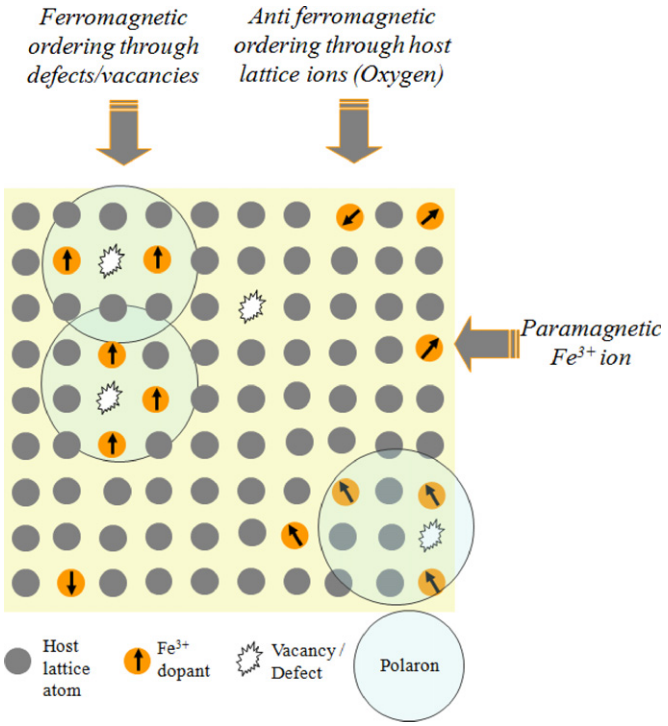

Fig. 12. Schematic representation of Fe doped ZnO.

4. Conclusions

In summary, the microwave-assisted synthesis of ZnO and Fe doped ZnO nanorods with high aspect ratio ($\sim$1 μm average length and $\sim$50 nm diameter) have been obtained. The structure of the sample is wurtzite with no impurity phases. The photoluminescence quenching is observed as Fe doping percentage increases. This has been attributed to the non-radiative recombination due to Fe trapping centers. Presence of high spin Fe^{3+} ions in the lattice is confirmed from the ESR and Mössbauer analysis. RTFM has been observed in ZnO nanorods with magnetization $\sim 5 \times 10^{-3}$ emu/g and coercivity $\sim$150 Oe. The origin of ferromagnetism in undoped ZnO nanorods is attributed to surface defects/vacancies. Fe doped ZnO nanorods also show RTFM with T_c above 390 K. In Fe doped ZnO origin of ferromagnetism is explained by the F-center exchange (FCE) mechanism. The cumulative effect of ferromagnetic and paramagnetic/antiferromagnetic contribution gives rise to significant changes in M–H loop.

Acknowledgments

This work was supported by BRNS and DST India. SKK thanks UGC, MVL thanks BRNS and CSIR India and SBS thanks CSIR, India for financial support. Authors would like to thank Dr. N.P. Lalla, UGC-DAE Consortium for Scientific Research, Indore 452017, India and Saurabh Gosh and Dr. G.P. Das, IACS, Kolkata, for TEM analysis; and SAIF, IITB, India for ESR analysis. Authors would like to thank Dr. S.K. Date for valuable suggestions. One of the authors PP would like to acknowledge support from the DST, India through the grant no. SR/S5/NM-104/2006) under the "Nano Mission" programme.

Appendix A. supplementary Materials

Supplementary data associated with this article can be found in the online version at doi:10.1016/j.jssc.2010.11.008.

References

[1] J.K. Furdyna, J. Appl. Phys. 64 (1988) R29.
[2] H. Ohno, Science 281 (1998) 951.
[3] S.A. Wolf, D.D. Awschalom, R.A. Buhrman, J.M. Daughton, S. von Molnar, M.L. Roukes, A.Y. Chtchelkanova, D.M. Treger, Science 294 (2001) 1488.
[4] M. Johnson, J. Phys. Chem. B 109 (2005) 14278.
[5] H. Ohno, A. Shen, F. Matsukura, A. Oiwa, A. Endo, S. Katsumoto, Y. Iye, Appl. Phys. Lett. 69 (1996) 363.
[6] J.M.D. Coey, M. Venkatesan, C.B. Fitzgerald, Nat. Mater. 4 (2005) 173.
[7] J.M.D. Coey, A.P. Douvalis, C.B. Fitzgerald, M. Venkatesan, Appl. Phys. Lett. 84 (2004) 1332.
[8] Z.J. Wang, J.K. Tang, L.D. Tung, W.L. Zhou, L. Spinu, J. Appl. Phys. 93 (2003) 7870.
[9] N.Y.H. Hong, J. Sakai, A. Hassini, Appl. Phys. Lett. 84 (2004) 2602.
[10] Marcel H.F. Sluiter, Y. Kawazoe, P. Sharma, A. Inoue, A.R. Raju, C. Rout, U.V. Waghmare, Phys. Rev. Lett. 94 (2005) 187204.

[11] S.-J. Han, J.W. Song, C.-H. Yang, S.H. Park, J.-H. Park, Y.H. Jeong, K.W. Rhie, Appl. Phys. Lett. 81 (2002) 4212.
[12] X.X. Wei, C. Song, K.W. Geng, F. Zeng, B. He, F. Pan, J. Phys.: Condens. Mater. 18 (2006) 7471.
[13] D. Karmakar, S.K. Mandal, R.M. Kadam, P.L. Paulose, A.K. Rajarajan, T.K. Nath, A.K. Das, I. Dasgupta, G.P. Das, Phys. Rev. B 75 (2007) 144404.
[14] A. Singhal, S.N. Acharya, A.K. Tyagi, P.K. Manna, S.M. Yusuf, Mater. Sci. Eng. B 153 (2008) 47.
[15] B.K. Roberts, A.B. Pakhomov, V.S. Shutthanandan, K.M. Krishnan, J. Appl. Phys. 97 (2005) 10D310.
[16] A. Tiwari, M. Snure, D. Kumar, J.T. Abiade, Appl. Phys. Lett. 92 (2008) 062509.
[17] P. Sharma, A. Gupta, K.V. Rao, F.J. Owens, R. Sharma, R. Ahuja, J.M.O. Guillen, B. Johansson, G.A. Gehring, Nature Mater. 2 (2003) 673.
[18] X.X. Lin, Y.F. Zhu, W.Z. Shen, J. Phys. Chem. C 113 (2009) 1812.
[19] M. Diaconu, et al., Thin Solid Films 486 (2005) 117.
[20] K.R. Kittilstved, D.R. Gamelin, J. Am. Chem. Soc. 127 (2005) 52932.
[21] X. Wang, J. Xu, B. Zhang, H. Yu, J. Wang, X. Zhang, J. Yu, Q. Li, Adv. Mater. 18 (2006) 2476.
[22] C. Song, K.W. Geng, F. Zeng, X.B. Wang, Y.X. Shen, F. Pan, Y.N. Xie, T. Liu, H.T. Zhou, Z. Fan, Phys. Rev. B 73 (2006) 024405.
[23] X. Wang, J.B. Xu, W.Y. Cheung, J. An, N. Ke, Appl. Phys. Lett. 90 (2007) 212502.
[24] M.V. Limaye, S.B. Singh, S.K. Date, R.S. Gholap, S.K. Kulkarni, Mater. Res. Bull. 44 (2009) 339.
[25] Z.H. Zhang, X. Wang, J.B. Xu, S. Muller, C. Ronning, Quan Li, Nat. Nanotech. 4 (2009) 523.
[26] C.N.R. Rao, F.L. Deepak, J. Mater. Chem. 15 (2005) 573.
[27] M.S. Seehra, P. Dutta, S. Neeleshwar, Y.-Y. Chen, C.L. Chen, S.W. Chou, C.C. Chen, C.-L. Dong, C.-L. Chang, Adv. Mater. 20 (2008) 1656.
[28] S.B. Singh, M.V. Limaye, S.K. Date, S.K. Kulkarni, Chem. Phys. Lett. 464 (2008) 208.
[29] C. Madhu, A. Sundaresan, C.N.R. Rao, Phys. Rev. B 77 (2008) 201306(R).
[30] M. Venkatesan, C.B. Fitzgerald, J.M.D. Coey, Nature 430 (2004) 630.
[31] M.A. Garcia, J.M. Merino, E.F. Pinel, A. Quesada, J. De la Venta, M.L.R. Gonzalez, G.R. Castro, P. Crespo, J. Llopis, J.M. G-callbet, A. Hernando, Nano Lett. 7 (2007) 1489.
[32] A. Sundaresan, R. Bhargavi, N. Rangarajan, U. Siddesh, C.N.R. Rao, Phys. Rev. B 74 (2006) 161306(R).
[33] V. Fernandes, et al., Phys. Rev. B 80 (2009) 035202.
[34] J. Hu, Z. Zhang, M. Zhao, H. Qin, M. Jiang, Appl. Phys. Lett. 93 (2008) 192503.
[35] C. Thelander, et al., Mater. Today 9 (2006) 28.
[36] U. Philipose, S.V. Nair, S. Trudel, C.F. de Souza, S. Aouba, R.H. Hill, H.E. Ruda, Appl. Phys. Lett. 88 (2006) 263101.
[37] K.F. Eid, B.L. Sheu, O. Maksimov, M.B. Stone, P. Schiffer, N. Samarth, Appl. Phys. Lett. 86 (2005) 152505.
[38] C. Xu, J. Chun, K. Rho, D.E. Kim, B.J. Kim, S. Yoon, S.-E. Han, J.-J. Kim, J. Appl. Phys. 99 (2006) 064312.
[39] W.B. Jian, Z.Y. Wu, R.T. Huang, F.R. Chen, J.J. Kai, C.Y. Wu, S.J.M. Chiang, D. Lan, J.J. Lin, Phys. Rev. B 73 (2006) 233308.
[40] X. Wang, R. Zheng, Z. Liu, H. Ho, J. Xu, S.P. Ringer, Nanotechnology 19 (2008) 455702.
[41] Y.R. Uum, B.S. Han, H.M. Lee, S.M. Hong, G.M. Kim, C.K. Rhee, Phys. Status Solidi (c) 4 (2007) 4408.
[42] S. Gautam, S. Kumar, P. Thakur, K.H. Chae, R. Kumar, B.H. Koo, C.G. Lee, J. Phys. D: Appl. Phys. 42 (2009) 175406.
[43] X. Wang, F. Song, T. Qian Chen, J. Wang, P. Wang, M. Liu, J. Shen, G. Wan, J.-B.Xu Wang, J. Am. Chem. Soc. 132 (2010) 6492.
[44] C.Y. Lin, W.H. Wang, C.-S. Lee, K.W. Sun, Y.W. Suen, Appl. Phys. Lett. 94 (2009) 151909.
[45] X.-W. Zhang, W.-J. Fan, Y.-H. Zheng, S.-S. Li, J.-B. Xia, Appl. Phys. Lett. 90 (2007) 253110.
[46] T. Yao, W. Yan, Z. Sun, Z. Pan, Y. Xie, Y. Jiang, J. Ye, F. Hu, S. Wei, J. Phys. Chem. C 113 (2009) 14114.
[47] S. Kumar, Y.J. Kim, B.H. Koo, S. Gautam, K.H. Chae, Ravi Kumar, C.G. Lee, Mater. Lett. 63 (2009) 194.
[48] T. Nobis, E.M. Kaidashev, A. Rahm, M. Lorenz, J. Lenzner, M. Grundmann, Nano Lett. 4 (2004) 797.
[49] W.I. Park, D.H. Kim, S.W. Jung, G.C. Yi, Appl. Phys. Lett. 80 (2002) 4232.
[50] M. Lai, D.Jason Riley, Chem. Mater. 18 (2006) 2233.
[51] M. Yin, Y. Gu, I.L. Kuskovsky, T. Andelman, Y. Zhu, G.F. Neumark, S. O'Brien, J. Am. Chem. Soc. 126 (2004) 6206.
[52] A.B. Panda, G. Glaspell, M.Samy El-Shall, J. Am. Chem. Soc. 128 (2006) 2790.
[53] M.V. Limaye, S. Gokhale, S.A. Acharya, S.K. Kulkarni, Nanotechnology 19 (2008) 415602.
[54] A. Singhal, S.N. Achary, J. Manjanna, O.D. Jayakumar, R.M. Kadam, A.K. Tyagi, J. Phys. Chem. C 113 (2009) 3600.
[55] D. Galland, A. Herve, Solid State Commun. 14 (1974) 953.
[56] A. Hausmann, Z. Phys. 237 (1970) 86.
[57] H. Zhou, A. Hofstaetter, D.M. Hofmann, B.K. Meyer, Microelectron. Eng. 66 (2003) 59.
[58] M. Jiang, J. Treea, A.M. Rossi, M.A. Morales, S.E.M. Baggio, D.E. Ellis, Phys. Rev. B 66 (2002) 114107.
[59] T.J. Caster, G.S. Newall, W.C. Holton, C.P. Slichter, J. Chem. Phys. 32 (1960) 668.
[60] P.H. Borse, N. Deshmukh, R.F. Shinde, S.K. Date, S.K. Kulkarni, J. Mater. Sci. 34 (1999) 6087.
[61] A.K. Singh, V. Viswanath, V.C. Janu, J. Lumin. 129 (2009) 874.
[62] C.X. Xu, X.W. Sun, X.H. Zhang, L. Ke, S.J. Chua, Nanotechnology 15 (2004) 856.
[63] E. De la Rosa, S. Sepúlveda-Guzman, B. Reeja-Jayan, A. Torres, P. Salas, N. Elizondo, M.Jose Yacaman, J. Phys. Chem. C 111 (2007) 8489.
[64] G.H. Du, F. Xu, Z.Y. Yuan, G.V. Tendeloo, Appl. Phys. Lett. 88 (2006) 243101.
[65] K. Vanheusden, W.L. Warren, C.H. Seager, D.R. Tallant, J.A. Voigt, B.E. Gnade, J. Appl. Phys. 79 (1996) 7983.
[66] Z. Yan, Y. Ma, D. Wang, J. Wang, Z. Gao, T. Song, J. Phys. Chem. C 112 (2008) 219.
[67] Y.-w. Jun, Y.-y. Jung, J. Cheon, J. Am. Chem. Soc. 124 (2002) 615.
[68] A. Parra-Palomino, O. Perales–Perez, R. Singhal, M. Tomar, J. Hwang, P.M. Voyles, J. Appl. Phys. 103 (2008) 07D121.
[69] S.B. Singh, M.V. Limaye, S.K. Date, S. Gokhale, S.K. Kulkarni, Phys. Rev. B 80 (2009) 235421.
[70] Z. Ren, G. Xu, X. Wei, Y. Liu, X. Hou, P. Du, W. Weng, G. Shen, G. Han, Appl. Phys. Lett. 91 (2007) 063106.
[71] S.-I. Park, G.Y. Ahn, C.S. Kim, J. Appl. Phys. 101 (2007) 09H113.
[72] Y. Sahoo, P. Poddar, H. Srikanth, D.W. Lucey, P.N. Prasad, J. Phys. Chem. B 109 (2005) 15221.
[73] P. Poddar, Y. Sahoo, H. Srikanth, P.N. Prasad, Appl. Phys. Lett. 87 (2005) 062506.
[74] Diandra L. Leslie-Pelecky, Reuben D. Rieke, Chem. Mater. 8 (1996) 1770 and references therein.
[75] C.B. Fitzgerald, M. Venkatesan, L.S. Dorneles, R. Gunning, P. Stamenov, J.M.D. Coey, Phys. Rev. B 74 (2006) 115307.
[76] T. Kasuya, Solid State Commun. 8 (1970) 1635.